Quantification of Chemical Pressure in Doped Nanostructured Zirconia Ceramics

Elisabeth Djurado,*,† Florence Boulc'h,† Guilhem Dezanneau,‡ and Pierre Bouvier†

Laboratoire d'Electrochimie et de Physico-Chimie des Matériaux et des Interfaces, Domaine Universitaire, INPG-CNRS-UJF, 1130 rue de la piscine, BP 75, 38402 St Martin d'Hères, France, and Dept Electronica, Universitat de Barcelona, Marti i Franquès, 1, E-08028 Barcelona, Spain

Received: January 16, 2003; In Final Form: May 23, 2003

The influence of the substitution of Zr^{4+} by oversized rare-earth R^{3+} ($R \simeq$ Sc, Yb, Y, Gd, Sm) was investigated in nanocrystalline tetragonal R_2O_3-doped zirconia (ZrO_2) ceramics. Three batches of samples were investigated as a function of various contents of oversized trivalent dopants, i.e., (i) scandia and (ii) ytterbia, and as a function of different dopant ionic radii, for a constant R_2O_3 content of 3 mol %. Quantification of internal pressure was performed from frequency shifts of Raman spectra and from compressibility data from XRD.

Introduction

Nanostructured tetragonal zirconia polycrystalline (TZP) material challenges the well-known yttria-stabilized zirconia (YSZ) solid electrolyte due to its confirmed high ionic conductivity[1−4] at intermediate temperature up to 750 °C and to its relevant mechanical properties.[5] Thus, TZP could be considered as a good candidate to be used as an electrolyte in solid oxide fuel cells operating at intermediate temperature (IT-SOFCs).

High-temperature tetragonal zirconia (ZrO_2) can be stabilized at room temperature (RT) if different oxides such as rare earth oxides are added[6] and/or if a nanometric grain size is maintained.[7] The doping of zirconia by lower valence cations leads to (i) an increase of the number of oxygen ion vacancies, which consequently favors an enhancement of the ionic conductivity, since they are mobile, (ii) structural changes from monoclinic, tetragonal to cubic phases, and (iii) local strains due to short-range interaction between Zr^{4+} and its dopant, which are expected to be a function of the dopant ionic radius size.[8]

It has been well-established that the substitution of different size ions into a cationic site exerts a "chemical pressure" on the system. Usually, the chemical pressure effects have been put into evidence following the evolution of some specific properties in relationships with the average dopant ionic radius. For instance, magnetoresistance was found tunable by doping either Ca or Ba into the Sr site in $SrFe_{0.5}Mo_{0.5}O_3$[9] or by substituting different rare-earth ions for La in $LaMnO_3$.[10,11] It was also shown that superconducting properties were strongly related to the substitution of Sr for Ba in the YBCO system.[12] Karpinski[13] et al. have recently investigated the influence of substitution of Sr for Ba in superconducting cuprates on the structure using X-ray diffraction. They showed from a macroscopic point of view that this doping has induced both increase of hole concentration in Cu in the planes and contraction of lattice parameters equivalent to an application of about 2.2 GPa hydrostatic pressure for a substitution of 30% Ba with Sr. Up to now, no data were available in the literature about the quantitative determination of internal stresses using a microscopic probe such as Raman spectroscopy.

Very recently, we have reported[14] the structural changes in nanometric R_2O_3-doped ZrO_2 ceramics (R = Sc, Yb, Y, Gd, Sm) as a function of the dopant content and ionic radius using both X-ray diffraction and Raman spectroscopy. In the present work, Raman and X-ray diffraction data are analyzed in order to put into evidence, for the first time, chemical pressures caused by substitution of zirconium cation by oversized trivalent dopants in zirconia matrix using both complementary characterization techniques: a local probe such as Raman spectroscopy and a macroscopic one such as X-ray diffraction.

This paper describes a quantification of internal stresses in nanocrystalline zirconia ceramics due to the doping of Zr^{4+} by trivalent oversized dopant using Raman spectroscopy first and X-ray diffraction second for three different series: as a function of Sc^{3+} dopant content, as a function of Yb^{3+} dopant content, and as a function of the dopant size for a constant dopant content (3 mol % R_2O_3, $R \simeq$ Yb, Y, Gd, Sm).

Experimental Section

Preparation of Doped Nanostructured Ceramics. Rare-earth oxide dopants were selected for their lower valence (+3) compared to Zr^{4+} and for a systematic increase in their ionic radii ranging from 0.087 to 0.109 nm, respectively, from Sc^{3+} to Sm^{3+}. Doped nanocrystalline powders of $(ZrO_2)_{1-x}(R_2O_3)_x$ with 0.03 mol $\leq x \leq$ 0.09 mol final content of Sc_2O_3, Yb_2O_3, Y_2O_3, Gd_2O_3, and Sm_2O_3 were synthesized by ultrasonic-assisted spray pyrolysis.[15] This method involved the pyrolysis at 600 °C in a tubular furnace of an aerosol that consisted of metal nitrates dissolved in deionized water with a 2.5×10^{-2} mol L^{-1} concentration. One advantage of this one-step synthesis was to obtain dense and compositionally homogeneous nanocrystalline powders of doped zirconia, at low temperature in which no amorphous phase was detected by either XRD or Raman spectroscopy. An average crystallite size of 6 nm for all samples was calculated by the Scherrer formula from X-ray diffraction patterns and was coherent with high-resolution transmission electron microscopy (HRTEM) observations.[16] In a second step, these spray-pyrolysis powders were compacted by cold isostatic pressing at 300 MPa and subsequently sintered at 1500 °C for 2 h in air. The final stoichiometry of the pellets

* Corresponding author. Phone 33-4-76826684. Fax: 33-4-76826777. E-mail address: Elisabeth.Djurado@lepmi.inpg.fr.
† Domaine Universitaire.
‡ Universitat de Barcelona.

10.1021/jp0341220 CCC: $25.00
Published on Web 07/22/2003

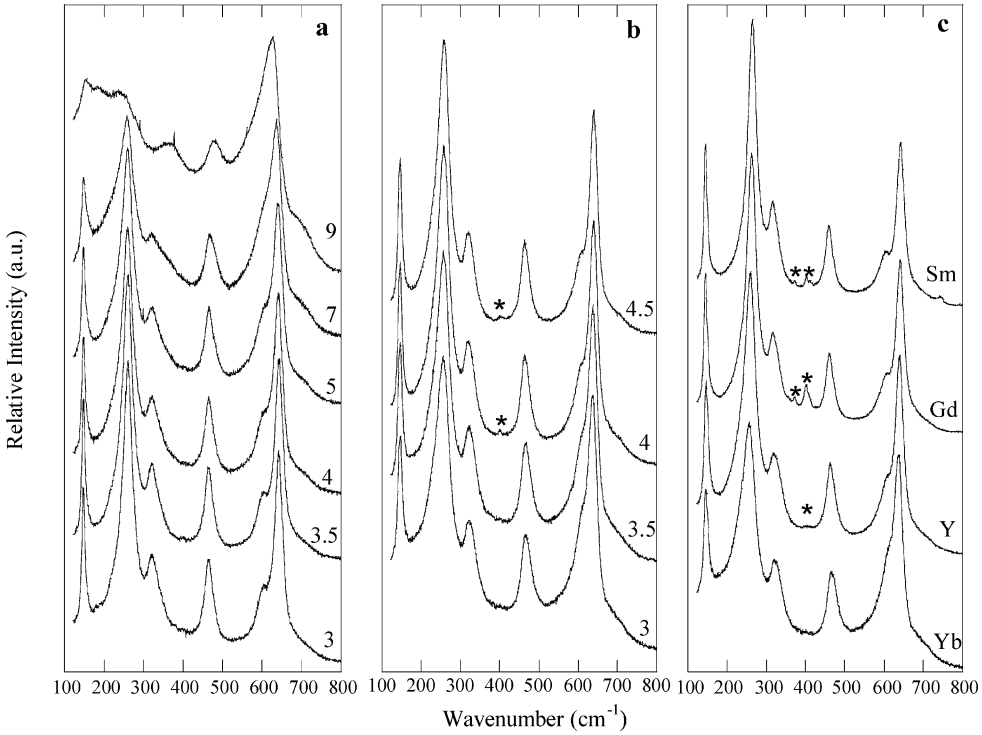

Figure 1. Raman spectra of (a) *x* mol % Sc_2O_3-doped ZrO_2, (b) *x* mol % Yb_2O_3-doped ZrO_2, (c) 3 mol % R_2O_3-doped ZrO_2 (R = Yb, Y, Gd, Sm). *: fluorescence.

was determined by electron probe microanalysis (CAMECA SX, 50, 200 nA, 15 kV) using $(ZrO_2)_{0.92}(Y_2O_3)_{0.08}$ as standard. All ceramics were characterized by the same microstructure, whatever the nature and concentration of the dopants were. Indeed, an average grain size as low as 60 nm and densities as high as 96% of the theoretical values were measured. It is therefore expected that variations of Raman spectra will not be due to microstructural contributions but will mainly depend on the nature of the dopant and its content.

Characterization Techniques. X-ray diffraction was performed at room temperature using a Siemens $\theta/2\theta$ D500 diffractometer equipped with a linear detector (Cu Kα radiation, $\lambda = 1.5406$ Å, 0.004°, 2θ steps, 5 s counting time). The cell parameters (*a* and *c*) of the tetragonal form were refined in the $P4_2/nmc$ space group. The reflection positions were determined by fitting peaks with a pseudo-Voigt function, the parameters of which vary according to a modified Cagliotti's resolution function.

Room-temperature micro-Raman spectra were recorded using a DILOR XY multichannel spectrometer equipped with a CCD detector cooled by liquid nitrogen. The 514.53 nm excitation line of an argon ion laser was used. The position and intensity of Raman bands were obtained by the deconvolution of Lorentzian-shaped peaks with the PeakFit software (v. 4.0, Jandel Scientific). Wavenumber accuracy was estimated to about 0.1 cm^{-1} using monoclinic ZrO_2 as standard reference. We performed quantitative XRD and Raman analyses of tetragonal/monoclinic/cubic forms using the same procedure as was previously performed for t/m and t/c mixtures in doped nanometric zirconia.[14]

Results

Figure 1 shows Raman spectra of three different batches of nanostructured ZrO_2 ceramics that all present the same microstructure (4% porosity, 60 nm grain size), whatever the nature of the dopant and its concentration are: (a) $(ZrO_2)_{1-x}(Sc_2O_3)_x$ with 0.03 mol $\leq x \leq$ 0.09 mol final content, (b) $(ZrO_2)_{1-x}(Yb_2O_3)_x$ with 0.03 mol $\leq x \leq$ 0.045 mol final content, (c) 3 mol % R_2O_3-doped ZrO_2, (R $\simeq$ Yb, Y, Gd, Sm). In Sm-, Yb-, and Gd-doped ZrO_2, peaks due to fluorescence of rare-earth cations were observed near 400 cm^{-1} (designated with an * in Figure 1). They will not be considered further in this study. The contents of monoclinic, tetragonal, and cubic zirconia polymorphs are reported in Table 1 versus R dopant ionic size and R_2O_3 dopant content. The presence of two phases, tetragonal/monoclinic for lower dopant content and tetragonal/cubic for higher dopant contents, was obtained in the Sc_2O_3-doped ZrO_2 series, except for the composition at 3.5 mol %, which corresponds to the tetragonal single-phased solid solution. In the following, samples that contain a Sc_2O_3 content superior to 5 mol % will not be considered in the quantitative determination of the chemical pressure. All other R_2O_3-doped ZrO_2 ceramics (R = Yb, Y, Gd, Sm) were tetragonal single-phased.

TABLE 1: Monoclinic (M)/Tetragonal (T)/Cubic (C) Zirconia Polymorphs versus R Dopant Ionic Size and Dopant Content (mol % R_2O_3) Measured at Room Temperature in Ceramics Sintered at 1500 °C/2 h in Air

dopant content (R_2O_3 mol %)	Sc^{3+} 0.087 nm	Yb^{3+} 0.098 nm	Y^{3+} 0.102 nm	Gd^{3+} 0.106 nm	Sm^{3+} 0.109 nm
3	T + 5% M	T	T	T	T
3.5	T	T			
4	T +40% C	T			
4.5		T			
5	T + 60% C				
7	T + 80% C				
9	T + 95% C				

Quantitative Determination of Chemical Pressure from Raman Frequency Shifts. Frequency shifts of all six Raman bands characteristic of tetragonal ZrO_2 were found to vary continuously with R_2O_3 content and with the size of the dopant cation (at fixed 3 mol % content of different R_2O_3 dopants: R $\simeq$ Yb, Y, Gd, Sm) (Figure 2). Experimental values of frequency variations between the lowest and the highest dopant content

TABLE 2: Measured and Extrapolated Frequency Shifts ($\Delta\nu$) of the Six Raman Modes of t-ZrO_2 Spectra, Pressure-Dependence of Raman Band Frequencies (g), and Chemical Pressure for Three Series

(a) Frequency Shifts for Sc-TZP

ν (cm^{-1})	measured $\Delta\nu$ (cm^{-1}) from 3 to 5 Sc-TZP	g (cm^{-1}/GPa)	measured P_c (GPa)	extrapolated $\Delta\nu$ (cm^{-1}) from 0 to 5 Sc-TZP	extrapolated P_c (GPa)
150	0.5	1.8	0.3	1.2	0.7
260	−1.7	−3.6	0.5	−4.3	1.2
320	3.1	3.4	0.9	7.8	2.3
460	1.4	5.6	0.3	3.5	0.6
600	4.0	2.4	1.7	10.0	4.2
640	−2.3	2.8	−0.8		

(b) Frequency Shifts for Yb-TZP

ν (cm^{-1})	measured $\Delta\nu$ (cm^{-1}) from 3 to 4.5 Yb-TZP	g (cm^{-1}/GPa)	measured P_c (GPa)	extrapolated $\Delta\nu$ (cm^{-1}) from 0 to 4.5 Yb-TZP	extrapolated P_c (GPa)
150	−0.7	1.8	−0.4	−2.1	−1.2
260	3.7	−3.6	−1.0	11.1	−3.1
320	−4.6	3.4	−1.3	−13.8	−4.1
460	−3.6	5.6	−0.7	−10.8	−1.9
600	−7.1	2.4	−3.0	−21.3	−8.9
640	2.6	2.8	0.9		

(c) Frequency Shifts for 3R-TZP

ν (cm^{-1})	measured $\Delta\nu$ (cm^{-1}) from 3R-TZP (R = Yb, Y, Gd, Sm)	g (cm^{-1}/GPa)	measured P_c (GPa)
150	−1.4	1.8	−0.8
260	11.7	−3.6	−3.3
320	−8.6	3.4	−2.5
460	−8.4	5.6	−1.5
600	−11.1	2.4	−4.6
640	5.1	2.8	1.8

and for the third series between the smallest and the largest ionic radii are reported in Table 2. In the Sc series, lines at 150, 320, 460, and 600 cm^{-1} are shifted toward higher frequencies when dopant content is increased, while the lines at 260 and 640 cm^{-1} are inversely shifted toward lower frequencies. On the contrary, opposite frequency shifts are observed for the same two groups of Raman bands when Yb content is increased in the Yb series and when the dopant radius is increased at fixed 3 mol % doping level.

Raman frequency shifts were previously calibrated for compressive pressures up to 10 GPa in nanometric (18 nm) undoped ZrO_2,[17] which can be considered as representative of the undoped tetragonal matrix. It was shown that under compressive stresses all Raman bands are shifted toward higher frequencies, except for the 260 cm^{-1} band, which shifts toward lower frequencies. In the case of Sc-doped ZrO_2, we observe the same tendency for the first five Raman lines. The behavior of the 640 cm^{-1} band is not compatible with such a pressure effect. This will be developed in the following discussion part.

Using these calibrated data, an equivalent pressure quantification induced by doping, which can also be called a chemical "internal pressure", was undertaken in these ceramics as a function of dopant concentration and dopant size. The chemical pressure P_c was quantified using the following formula: $P_c = \Delta\nu/g$, where $\Delta\nu$ corresponds to measured frequency shifts and g is the calibrated pressure dependence of the Raman bands frequency. These g coefficients correspond to conditions of nearly ideal hydrostatic pressures. They are listed in Table 2 along with all experimental values. An average compressive chemical pressure of 0.7 GPa can be obtained from the average of each pressure measured on each Raman line at 140, 260, 320, 420, and 600 cm^{-1}, when the content of Sc is increased from 3 to 5 mol % Sc_2O_3-doped zirconia (Figure 3a, Table 2a).

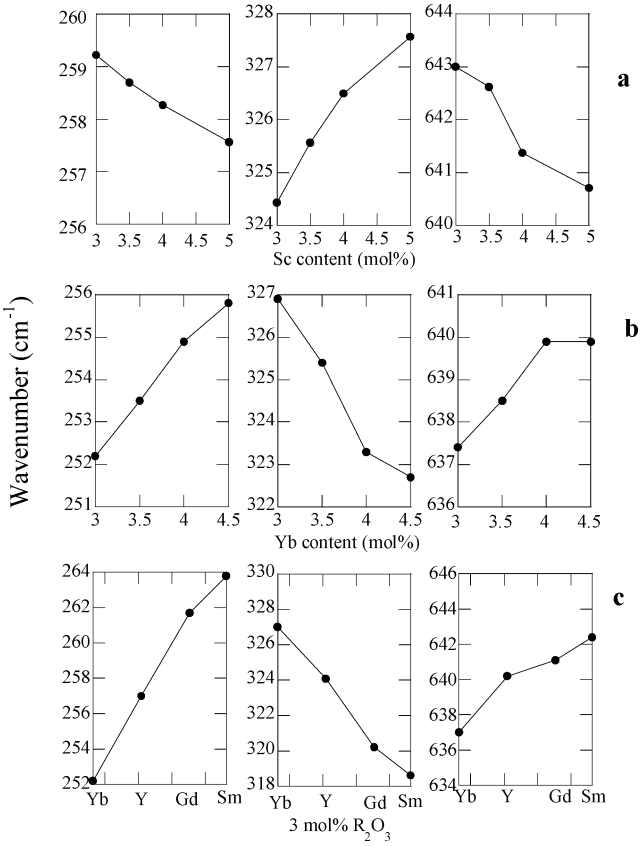

Figure 2. Raman frequencies of 260, 320, and 640 cm^{-1} versus (a) Sc content, (b) Yb content, and (c) dopant size for 3 mol % R_2O_3 (R ≃ Yb, Y, Gd, Sm). It is worth noting that molar masses are 173 g mol^{-1} for Yb, 89 g mol^{-1} for Y, 157 g mol^{-1} for Gd, 150 g mol^{-1} for Sm.

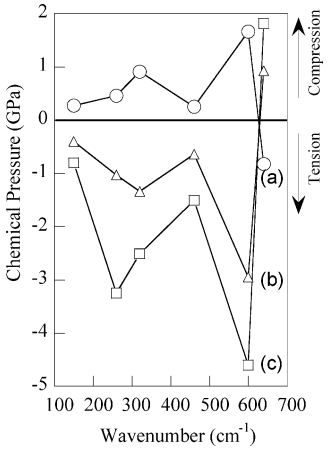

Figure 3. Chemical pressure in absolute values for the six tetragonal zirconia Raman modes versus (a) Sc content increase from 3 to 5 mol %, (b) Yb content increase from 3 to 4.5 mol %, (c) dopant size for 3 mol % R_2O_3 (R ≃ Yb, Y, Gd, Sm). Compressive and tensile domains are indicated by arrows.

The tensile pressure of 1.3 GPa on average was determined when the content of a larger oversized dopant Yb^{3+} (0.098 nm) was increased from 3 to 4.5 mol % Yb_2O_3-doped zirconia (Figure 3b, Table 2b).

Taking into account that these evolutions were found to be linear, as shown in Figure 2, it is possible to extend the domain to pure tetragonal zirconia. For instance, an average equivalent compressive chemical pressure of 1.8 GPa in the 0 to 5 mol % Sc_2O_3 domain (see Table 2a) and an average equivalent tensile pressure of 3.8 GPa in the 0 to 4.5 mol % Yb_2O_3 domain (see Table 2b) were calculated by extrapolation. It is worth noting that frequency positions determined by extrapolation are similar to those previously measured on pure 18 nm tetragonal ZrO_2.[17] Notice that ZrO_2 can be considered as similar to bulk tetragonal ZrO_2. Indeed, we have previously demonstrated that Raman frequency shifts that can be induced by confinement because of small size are only observed for grain size below 10 nm.[7]

Larger tensile stresses were found equal to 2.5 GPa on average when the dopant ionic radius size is increased from 0.098 nm (Yb^{3+}) to 0.109 nm (Sm^{3+}) (Figure 3c, Table 2c). In this case, the reference was selected as the tetragonal single-phased specimen that contained the smallest dopant ionic radius, i.e., 3Yb doped-TZP.

Quantitative Determination of Chemical Pressure from X-ray Diffraction. Evolution of the cell parameters of the tetragonal structure was obtained for the same samples using X-ray diffraction. When the dopant concentration is increased from 3 to 5 mol % Sc_2O_3-doped zirconia, the *a* lattice parameter is found to be constant and *c* is slightly decreased. The tetragonality defined as the *c*/*a* ratio (Figure 4a, Table 3) is slightly decreased.

When the content of a larger oversized dopant Yb^{3+} (0.098 nm) is increased from 3 to 3.5, to 4, to 4.5 mol % Yb_2O_3-doped ZrO_2, the *a* lattice parameter is slightly decreased while the *c* parameter is slightly increased, leading to a noticeable increase of the *c*/*a* ratio (Figure 4a, Table 3). It seems that the steric effect, due to the ionic radius difference between Zr^{4+} and Yb^{3+} when the substitution of Zr^{4+} by Yb^{3+} occurs, mainly governs the increase of the *c*/*a* ratio in favor of a larger tetragonality.

As far as the dopant size is increased in single-phased tetragonal zirconia solid solutions characterized by a constant dopant content (3 mol % R_2O_3; R ≃ Yb, Y, Gd, Sm), the *c* lattice parameter is strongly increased. Simultaneously, the *a* lattice parameter is almost constant, leading to a considerable increase of the *c*/*a* ratio (Figure 4b, Table 3), as an indicator of a better stability of the tetragonal form of zirconia. From these data, it is concluded that the *c* lattice parameter is strongly dependent on the cationic size. These results are consistent with our previous work[18] based a on high-pressure X-ray diffraction study on pure nanometric ZrO_2. In this study, linear compressibilities along tetragonal crystallographic axes were measured by X-ray diffraction and found to be higher for the *c* axis than for the *a* axis in the pressure range lower than 8 GPa. It was demonstrated that the tetragonal structure is softer along this *c* direction. Let us calculate the equivalent pressures in the three series deduced from XRD data.[18] From the linear compressibility $\beta_c = 2.24(6) \times 10^{-12}$ Pa^{-1} found along *c* axis, we have calculated compressive stresses of 1.1 GPa for the scandia series ($\Delta P = -\Delta c/c \times 1/\beta_c$). Tensile stresses of 0.8 and 2.6 GPa were respectively found for the ytterbia series and for the fixed 3 mol % R_2O_3-doped ZrO_2 when the dopant ionic radius is increased from 0.098 nm (Yb^{3+}) to 0.109 nm (Sm^{3+}). The variations of the pressure that were measured in the *a* direction

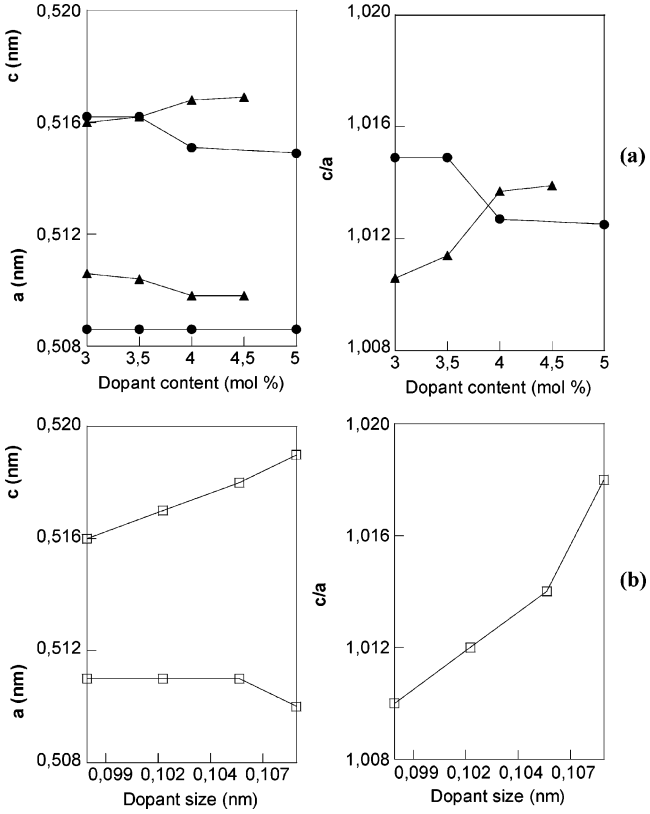

Figure 4. (a) *a* and *c* lattice parameters versus Sc content (●) and Yb content (▲), and *c*/*a* ratio versus Sc content (●) and Yb content (▲). (b) *a* and *c* lattice parameters and *c*/*a* ratio (□) versus 3 mol % R_2O_3 (R ≃ Yb, Y, Gd, Sm).

TABLE 3: Evolution of Tetragonal Lattice Parameters and of *c*/*a* Ratio versus Sc_2O_3 Content, Yb_2O_3 Content, and Dopant Size (3 mol % R_2O_3, R ≃ Yb, Y, Gd, Sm)[a]

	3 → 5 mol % Sc_2O_3	3 → 4.5 mol % Yb_2O_3	Yb → Sm 3 mol % R_2O_3
a_i (nm)	0.50851(3)	0.51062(4)	0.5107(4)
Δa (nm)	0.00002(10)	−0.0008(5)	0.0003(8)
c_i (nm)	0.51624(4)	0.51590(5)	0.5161(2)
Δc (nm)	−0.00124(5)	0.00106(8)	0.0027(3)
$(c/a)_i$	1.01520(7)	1.01034(9)	1.0106(6)
$\Delta(c/a)$	−0.00025(1)	0.00371(9)	0.0059(7)

[a] a_i, c_i, and $(c/a)_i$ correspond to initial values.

were found to be insignificant. These results are in very good agreement with the stresses determined from Raman frequency shifts.

Discussion

Before discussing induced stresses by trivalent doping in tetragonal zirconia, let us give some details on the competitive influence of dopant and vacancies on the Raman spectrum of tetragonal ZrO_2. The normal-mode analysis of t-ZrO_2[19] has shown that all Raman modes, except A_{1g}, involve both atomic masses of zirconium and oxygen and bond lengths such as ZrO_I and ZrO_{II}, which are the two types of bonds that define the local environment around each Zr cation.[20] Indeed, the A_{1g} mode is only related to oxygen displacements. Thus, the frequency of this mode should not be influenced by cationic masses but should be mainly governed by both ZrO_I and ZrO_{II} bonds, if we assume that the oxygen sublattice is maintained without any vacancies. The absence of vacancy is only satisfied when ZrO_2 is doped by tetravalent dopants. Kim et al.[21] have studied the effect of tetravalent dopants on the Raman spectra of t-ZrO_2. They have shown that the variation of the frequency of the Raman band at 260 cm^{-1} is mainly influenced by cation mass, whereas the frequency of the band at 640 cm^{-1} is governed by bond length. This gives strong support to the attribution of A_{1g} symmetry to the 640 cm^{-1} mode. The same attribution was obtained from a recent high-pressure experiment on undoped t-ZrO_2.[22] Note that there are still some controversies between various authors about the position of the totally symmetric A_{1g} mode in the Raman spectra of tetragonal ZrO_2.[23−25] In the case of trivalent cation doping, the assumption mentioned above about the conservation of the oxygen sublattice is not satisfied, because as the dopant amount is increased, the number of oxygen vacancies is also increased, due to charge compensation. In the case of varying the cation size for a constant dopant amount, the vacancy numbers remain constant and we might thus expect to be able to extract the effect of substitution of Zr cation by oversized dopant.

The present study has shown that precisely the shift of the Raman mode at 640 cm^{-1} is not correlated with other frequency shifts of all other modes in all series. For instance, when a compressive pressure is measured for the Sc^{3+}-doped ZrO_2 series, a tensile pressure is deduced for the 640 cm^{-1} mode. This might be due to the fact that this 640 cm^{-1} A_{1g} mode is very sensitive to a slight deformation of the short range oxygen sublattice around each cation. Indeed, it is well-known that higher frequency Raman modes are associated with shorter correlation length compared to lower frequency modes. Thus, this mode should be extremely sensitive to the distribution of oxygen vacancies around substitutional ions at a very short-range scale. Therefore, it is not too surprising to find such singular behavior.

Nevertheless, the fact that we observed coherent frequency shifts for all other Raman modes, either with increasing dopant amount or with increasing dopant size at fixed doping level whatever the cation mass is, means that, in the present case, the influence of cation mass is weak and can be neglected compared to bond lengths and lattice distortions. This is further supported by the fact that the dopant amounts considered in this study are low compared to the previous study (i.e. 20 mol % MO_2 with M = Ce^{4+}, Ti^{4+} in ref 21). Indeed, the average molar mass of zirconium and oxygen for 3 mol % Y_2O_3-doped zirconia are very close to that of pure ZrO_2, i.e., 91.08 g mol^{-1}compared to 91.22 g mol^{-1} in ZrO_2 for zirconium and 15.77 compared to 15.99 g mol^{-1} in ZrO_2 for oxygen.

The above results on internal pressure obtained from Raman frequency shifts are further supported by X-ray diffraction data, which bring more insight at long-range scale. When Zr^{4+} cation belonging to ZrO_2 matrix is substituted by oversized trivalent R^{3+} cations, tensile stresses should be always expected in the lattice due to the larger size and also to the smaller positive charge of the dopant. Actually, large tensile stresses were observed for oversized dopant such as Yb^{3+} when increasing the amount of doping element or when increasing the ionic radius of dopant in the 3 mol % R_2O_3-doped zirconia (R = Yb, Y, Gd, Sm). However, tensile stresses were not observed when the slightly oversized Sc^{3+} dopant was substituted for Zr^{4+} cation. On the contrary, compressive stresses were measured. In this case, where the ionic radius of the dopant is close to that of Zr^{4+}, the role of vacancies on local structural relaxations seems predominant. Indeed, recent ab initio calculations performed by Eichler[26] have shown that the introduction of a single vacancy in the t-ZrO_2 structure induces a displacement of all surrounding ions (oxygen and zirconium) toward the vacancy in order to reduce its size. Therefore, there is a competition from a steric point of view between vacancies and dopant size on the relaxation mechanism experienced by the structure. This compensation of the volume reduction by oxygen vacancies has been also reported by Ohta et al.[27] from sound velocity measurements in Ca- and Y-doped ZrO_2.

The competition between vacancy and dopant size on the mechanical relaxation of the structure might be also responsible of the vacancy trapping at some special position that is fully related to the conductivity of those materials. Indeed, it is well-known that, from experimental[28] and theoretical[29,30,26] investigations, oxygen vacancies prefer next nearest neighbor sites (with respect to the substitutional ion) over nearest neighbor sites in highly doped cubic zirconia. Moreover, Zacate[30] et al. have found that for dopant cation larger than Sc^{3+}, oxygen vacancies in a next nearest neighbor site are more strongly linked to the dopant (larger binding energies) as far as the trivalent dopant size is increased. However, the results found in this work are specific to zirconia-based materials and are not expected to be applicable to other fluorite structures, such as ceria-based materials,[31] where the binding energies of nearest neighbors and of next nearest neighbors were found to be on same order of magnitude.

Conclusions

Raman frequency shifts were used as a result of zirconia doping with oversized trivalent cations in order to quantify, for the first time, chemical pressure in nanocrystalline rare-earth (Sc, Yb, Y, Gd, Sm)-doped zirconia ceramics. Equivalent compressive stresses of about 0.7 GPa were found in Sc_2O_3-doped ZrO_2. Equivalent tensile stresses of about 1.3 GPa were found in tetragonal single-phased Yb_2O_3-doped ZrO_2 ceramics. The influence of increasing ionic radii (R = Yb, Y, Gd, Sm) on tetragonal single-phased R_2O_3-doped zirconia ceramics was the appearance of larger tensile stresses as high as about 2.5 GPa in the series for the same vacancy number. Coherent results are obtained using two complementary tools (X-ray diffraction and Raman spectroscopy) and show that tensile stresses are fully related to the expansion of the *c* lattice parameter due to the substitution of zirconium by oversized dopant for a constant vacancy content. It is a consequence of the softness of the tetragonal structure along its *c* axis. Moreover, we have demonstrated that the oxygen vacancy concentration strongly enters in competition with the cationic size of the dopant and especially when the misfit between zirconium and its dopant is small.

References and Notes

(1) Ramamoorthy, R.; Sundararaman, D.; Ramasamy, S. *Solid State Ionics* **1999**, *123*, 271−278.

(2) Cheikh, A.; Madani, A.; Touati, A.; Boussetta, H.; Monty, C. *J. Eur. Ceram. Soc.* **2001**, *21*, 1837−1841.

(3) Mondal, P.; Klein, A.; Jaegermann, W.; Hahn, H. *Solid State Ionics* **1999**, *118*, 331−339.

(4) Weppner, W. *Solid State Ionics* **1992**, *52*, 15−21.

(5) He, Y. J.; Winnubst, A.; Burggraaf, A. J.; Verweij, H.; van der Varst, P. G.; de With, B. G. *J. Am. Ceram. Soc.* **1996**, *79*, 3090−3096.

(6) Tsukuma, K.; Kubota, Y.; Tsukidate, T. *Advances in Ceramics Science and Technology of Zirconia II*; Claussen, N., Ruehle, M., Heuer, A. H., Eds.; The American Ceramic Society Inc.: Columbus, OH, 1984; Vol. 12, p 382.

(7) Djurado, E.; Bouvier, P.; Lucazeau, G. *J. Solid State Chem.* **2000**, *149*, 399−407.

(8) Nakajima, A.; Ishigame, M. *Solid State Ionics* **2002**, *146*, 133−141.

(9) Kim, B.-G.; Hor, Y.-S.; Cheong S.-W. *Appl. Physics Lett.* **2001**, *79* [3], 388−390.

(10) Hwang, H. Y.; Palstra, T. T. M.; Cheong S.-W.; Batlogg, B. *Phys. Rev. B* **1995**, *52*, 15046−15049.

(11) Hwang, H. Y.; Cheong S.-W.; Radaelli, P. G.; Marezio, M.; Batlogg, B. *Phys. Rev. Lett.* **1995**, *75*, 914−917.

(12) Marezio, M.; Licci, F.; Gauzzi, A. *Physica C* **2000**, *337*, 195−199.

(13) Karpinski, J.; Kazakov S. M.; Angst, M.; Mironov, A.; Mali, M.; Roos, J. *Phys. Rev. B* **2001**, *64*, 094518.

(14) Boulc'h, F.; Djurado, E. *Solid State Ionics* **2003**, *157*, 335−340.

(15) Djurado, E.; Meunier, E. *J. Solid State Chem.* **1998**, *141*, 191−198.

(16) Boulc'h, F.; Schouler, M. C.; Donnadieu, P.; Chaix, J.-M.; Djurado, E. *J. Stereol. Image Anal.* **2001**, *20*, 157−161.

(17) Bouvier, P.; Lucazeau, G. *J. Phys. Chem. Solids* **2000**, *61*, 569−578.

(18) Bouvier, P.; Djurado, E.; Lucazeau, G.; Le Bihan T. *Phys. Rev. B* **2000**, *62*, 8731−8737.

(19) Bouvier, P.; Gupta, H. C.; Lucazeau, G. *J. Phys. Chem. Solids* **2001**, *62*, 873−879.

(20) Teufer, G. *Acta Crystallogr.* **1962**, *15*, 1187.

(21) Kim, D.-J.; Jang, J.-W.; Lee, H.-L. *J. Am. Ceram. Soc.* **1997**, *80*, 1453−1461.

(22) Bouvier, P.; Dmitriev, V. P.; Lucazeau, G. *Phys. Rev. B* Submitted.

(23) Feinberg, A.; Perry, C. H. *J. Phys. Chem. Solids* **1981**, *42* (6), 512−518.

(24) Mirgorodsky, A. P.; Smirnov, M. B.; Quintard, P. E. *J. Phys. Chem. Solids* **1999**, *60*, 985−992.

(25) Merle, Th.; Guinebretiere, R.; Mirgorodsky, A.; Quintard, P. *Phys. Rev. B* **2002**, *65*, 144302.

(26) Eichler, A. *Phys. Rev B.* **2001**, *64*, 174103.

(27) Ohta, M.; Wigmore, J. K.; Nobugai, K.; Miyasato, T. *Phys. Rev B.* **2002**, *65*, 174108.

(28) Argyriou, D. N.; Elcombe, M. M.; Larson, A. C. *J. Phys. Chem. Solids* **1996**, *57*, 183−193.

(29) Khan, M. S.; Islam, M. S.; Bates, D. R. *J. Mater. Chem.* **1998**, *8* (10), 2299−2307.

(30) Zacate, M. O.; Minervini, L.; Bradfield, D. J.; Grimes, R. W.; Sickafus, K. E. *Solid State Ionics* **2000**, *128*, 243−254.

(31) Minervini, L.; Zacate, M. O.; Grimes, R. W. *Solid State Ionics* **1999**, *116*, 339−349.